Electronic Supplementary Material (ESI) for Materials Advances.

Supporting Information

Unraveling the Compositional Heterogeneity and Carrier Dynamics of Alkali Cation Doped 3D/2D Perovskites with Improved Stability

Ming-Chun Tang[a,b,c‡], Siyuan Zhang[a,d‡], Timothy J. Magnanelli[a], Nhan V. Nguyen[a], Edwin J. Heilweil[a], Thomas D. Anthopoulos[b*] and Christina A. Hacker[a*]*

[a]Physical Measurement Laboratory, National Institute of Standards and Technology (NIST), Gaithersburg, MD 20899, USA

[b]King Abdullah University of Science and Technology (KAUST), KAUST Solar Center (KSC), and Physical Science and Engineering Division (PSE), Thuwal, 23955-6900, Saudi Arabia

[c]Institute for Research in Electronics and Applied Physics & Maryland NanoCenter, University of Maryland, College Park, MD 20742, USA

[d]Theiss Research, La Jolla, CA 92037, USA

[‡] M.-C. Tang and S. Zhang contributed equally to this work.

AUTHOR INFORMATION

Corresponding Author

* Email: mingchun.tang@nist.gov; thomas.anthopoulos@kaust.edu.sa;

chistina.hacker@nist.gov

Experimental Section

Materials, perovskite precursor solutions preparation, and deposition protocol

Materials preparation: Lead (II) iodide (PbI_2, 99.99%), lead (II) bromide ($PbBr_2$, 99.99%), formamidine iodide (FAI), methylammonium bromide (MABr), phenethylammonium iodide (PEAI), and rubidium iodide (RbI, 99.9%) were purchased from Sigma-Aldrich. The solvents dimethyl sulfoxide (DMSO, 99.8%), N,N-dimethylformamide (DMF, 99.8%), isopropyl alcohol (IPA, anhydrous, 99.5%), and chlorobenzene (CB, anhydrous, 99.8%) were all purchased from Sigma-Aldrich and used without further purification.

Solution preparation and device fabrication: The precursor solution preparation was conducted under an inert atmosphere inside a nitrogen glove box. The $FA_{0.85-x}MA_{0.15}Rb_xPbI_{2.55}Br_{0.45}$ precursor solutions (1.2 M) were prepared with FAI, MABr, PbI_2, $PbBr_2$, and RbI dissolved in a solvent mixture of DMF and DMSO (4:1 volume ratio). For instance, the $FA_{0.8}MA_{0.15}Rb_{0.05}PbI_{2.55}Br_{0.45}$ precursor solution (1.2 M) was prepared with FAI (0.96 M), MABr (0.18 M), PbI_2 (1.014 M), $PbBr_2$ (0.186 M), and RbI (0.06 M) dissolved in a mixture of DMSO and DMF (4:1 volume ratio). For the $FA_{0.85-x}MA_{0.15}Rb_xPbI_{2.55}Br_{0.45}$ + $Pb(I_yBr_{1-y})_2$ solution, $Pb(I_yBr_{1-y})_2$ and ($FA_{0.85-x}MA_{0.15}Rb_x$) with the ratio of 1.1:1 were dissolved in the same solvent recipe. All perovskite solutions were filtered before use. The PEAI in IPA with various concentrations of 1, 5, and 10 mg/mL were prepared and stirred overnight at room temperature. The Spiro-OMeTAD (99.5%, p-OLED) solution was prepared by dissolving 90 mg spiro-OMeTAD, 18 µL lithium bis(trifluoromethanesulfonyl) imide (99 %, Acros Organics, 520 mg mL-1) in acetonitrile (99.7 %, Alfa Aesar), 30 µl cobalt dopant (Co TFSI salt, FK209, Anhydrous ACN Sigma Aldrich, the dopant solution prepared from 300 mg cobalt 3 in 1 ml ACN), and 30 µL 4-tert-butylpyridine (96 %, Aldrich) in 1 mL CB. The ITO-coated (2.4 cm × 2.4 cm) glass was cleaned by sequential sonication in acetone, isopropanol, and ethanol for 30 min each, then dried under clear airflow and treated with O_3 plasma for 16 min. The TiO_2 was prepared by chemical liquid phase deposition with a clean substrate immersed in a $TiCl_4$ (CP, Sinopharm Chemical Reagent Co., Ltd) aqueous solution with the volume ratio of $TiCl_4$:H_2O equal to 9:400 at 70 °C for 55 min. The spin coating was accomplished inside a nitrogen glove box. For 3D perovskite films, perovskite solutions were spin-

coated on top of the TiO_2 layer at 2000 rpm for 10s with an acceleration of 200 rpm/s. The second step was 4000 rpm for the needed time with a ramp-up of 1000 rpm/s. Chlorobenzene (0.2 ml) was dropped on the spinning substrate during the second spin-coating step at 10s before the end of the procedure. The films were then thermally annealed at 100 °C for 10 min. For the 3D/2D perovskite film, the $FA_{0.85-x}MA_{0.15}Rb_xPbI_{2.55}Br_{0.45}$ + $Pb(I_yBr_{1-y})_2$ precursor solution was first spin-coated and annealed following the same procedure as for the 3D perovskite film. 50 μL of various concentrations PEAI in IPA was cast on the thermally annealed $FA_{0.85-x}MA_{0.15}Rb_xPbI_{2.55}Br_{0.45}$ + $Pb(I_yBr_{1-y})_2$ film during spin-coating at 3000 rpm for 30 s, followed by thermal annealing at 100 °C for 3 min. Subsequently, the Spiro-OMeTAD was deposited as the hole transporting layer on the top of perovskite by spin coating at 5000 rpm for 30 s followed by evaporation of 100 nm gold electrode on top of the cell.

Characterization

Optical metrology: UV-Vis data were acquired by the Carry 5000 UV-Vis NIR from 400 to 900 nm.

Electronic microscopy: SEM images were taken using NanoSEM with an in-lens detector using a 10 kV accelerating voltage and a 5 mm working distance.

Thickness measurement: The film thickness was confirmed by both the profilometry and spectroscopy ellipsometry (SE). The P-7 stylus profiler from Tencor is a surface measurement system with a 150 mm scan length standard. We used the P-7 stylus Tencor profiler to measure the thickness of hybrid perovskite thin films. SE measurements were performed in a chamber filled with nitrogen gas at room temperature on a vacuum ultraviolet spectroscopic ellipsometer consisting of Xenon and Deuterium lamps covering the wavelength from 140 nm to 1770 nm. The spectroscopic ellipsometer system used in this paper is J. A. Woollam (VUV-VASE VU-302), and photon energy ranges from 1.2 eV to 4.0 eV (with 0.01 eV step) during the measurement. The ellipsometry data, Ψ and Δ, was taken at 75° of incidence.

X-ray diffraction: XRD measurements were carried out in a θ-2θ configuration with a scanning interval of 2θ between 10° and 60° on a Brucker D8 (X-ray Source: Cu Kα; λ = 1.54 Å).

Solar cell characterizations: The current-density–voltage (*J–V)* curves were measured inside a nitrogen-filled glovebox by employing ABET solar simulator system with an illumination intensity of 1000 mW cm^{-2} (AM 1.5G), which calibrated via reference solar cell (RERA Technologies). The *J–V* curves were obtained by Keithley 2400 source, on an active area of 10 mm^2 was defined by a metal aperture to avoid light scattering from the metal electrode into a device during measurement for each pixel, without any pre-conditioning, at a scan rate of 300 mV s^{-1} in the voltage range from −0.1 to 1.2 V. The reversed scan (from 1.2 to −0.1 V) was reported for device hysteresis. The delay time was 50 ms, and the bias step was 0.02 V. Power output of the lamp was calibrated using an NREL-traceable KG5-filtered silicon reference cell. The EQE was characterized by a QTest Station 2000ADI system (Crowntech Inc., USA), and the light source was a 300 W xenon lamp. The monochromatic light intensity for the EQE measurement was calibrated with a reference silicon photodiode.

Time-resolved terahertz spectroscopy (TRTS): The TRTS apparatus is based on an amplified femtosecond laser system with 1 kHz repetition rate that has been described previously in detail.[1] TRTS is commonly employed to extract the photoconductivity and combined mobility of electron-hole pairs generated through photoexcitation in various materials. The terahertz (THz) probe pulse was produced by a 2 mm thick zinc telluride (ZnTe) <110> crystal to generate radiation from 0.5 THz to 2.0 THz. Residual 800 nm was filtered using a low-density foam filter and the cross-correlation time resolution of the excitation and probe pulse generated in this manner was ≈ 300 fs. The THz probe beam was collimated and focused onto the sample by two off-axis parabolic mirrors, the second of which has a hole drilled through its surface (just off-center) to allow for the pump beam to overlap at the sample. Dual lock-in amplifiers were utilized to simultaneously collect the ground state and photoinduced changes to the THz electric field, improving the time correlation between the complex quantities. 400 nm and 800 nm photoexcitation pulses were utilized to query locally higher density (≈ 38 nm penetration depth) and lower density (ca. homogeneous excitation) of the entire ca. 400 nm thickness of all the perovskite films, respectively.

Photoemission Spectroscopy Measurements: The 3D/2D mixed-cation lead mixed-halide perovskite films were transferred into the characterization chamber for ultraviolet and X-ray

photoemission spectroscopies (UPS and XPS) to determine the valence band levels and core levels. Angle-resolved XPS was also performed to study the elemental composition and access the layer's metal ion distribution. UPS and XPS Spectra were acquired on the Kratos Axis Ultra^{DLD} surface analysis system, using the He-I lamp radiation (21.2 eV) and monochromatic Al Kα line, respectively.[2] The films were characterized under a base pressure < 10^{-6} Pa. All samples were in electronic equilibrium with the spectrometer via a copper tape in contact with the perovskite film surface and characterized at a normal take-off angle unless stated otherwise. The Fermi level was calibrated using sputter cleaned gold film. Survey XPS scans were run at 160 eV pass energy and high-resolution scans at 20 eV pass energy. The UPS spectra were acquired at 5 eV pass energy and 0.05 eV step size with the aperture and iris set to 55 µm. From the binding energy corresponding to the SEE of the UPS spectra, we calculated the work function (ϕ = 21.22 eV – SEE) for each film, and from the onset of photoemission, we determine the position of the valence band maximum. XPS depth profiling was used to investigate the atomic composition at the bulk region using an Ar ion gun with power 1 kV and 600 nA on a raster area of 1 mm^2. The XPS spectra were collected after 150 s sputtering time. The sputtering rate is estimated to be 0.26 nm/s, assuming that the film thickness is 400 nm and it took 1500 s to etch through the film entirely. The film thickness of the films was measured by the profilometer and ellipsometry.

Supporting Data

Table S1. Summary of the band structure and energy levels for classic 2D, 3D, and 3D/2D bi-layer perovskites. The concentration of PEAI solution varies by 1 mg mL^{-1} (2D-1), 5 mg mL^{-1} (2D-5), and 10 mg mL^{-1} (2D-10) in isopropanol, respectively.

Perovskites	Band gap (eV)	E_f (eV)	$VBM - E_f$ (eV)	VBM (eV)	CBM (eV)
2D	2.34 ± 0.01	4.33 ± 0.03	1.58 ± 0.02	5.91 ± 0.04	3.57 ± 0.04
M0	1.59 ± 0.02	4.73 ± 0.03	1.28 ± 0.03	6.01 ± 0.05	4.43 ± 0.06
M0/2D-1	1.59 ± 0.01	4.65 ± 0.04	1.29 ± 0.02	5.94 ± 0.05	4.35 ± 0.05

M0/2D-5	1.58 ± 0.02	4.48 ± 0.05	1.49 ± 0.04	5.97 ± 0.06	4.38 ± 0.06
M0/2D-10	1.59 ± 0.02	4.42 ± 0.02	1.52 ± 0.02	5.94 ± 0.03	4.35 ± 0.04
Rb5	1.59 ± 0.01	4.53 ± 0.04	1.38 ± 0.03	5.91 ± 0.04	4.32 ± 0.05
Rb5/2D-1	1.59 ± 0.02	4.32 ± 0.02	1.46 ± 0.04	5.78 ± 0.05	4.19 ± 0.05
Rb5/2D-5	1.59 ± 0.02	4.28 ± 0.03	1.54 ± 0.05	5.82 ± 0.06	4.23 ± 0.05
Rb5/2D-10	1.59 ± 0.03	4.26 ± 0.04	1.58 ± 0.04	5.84 ± 0.06	4.25 ± 0.06

Table S2. Summary of the device parameters of 2D layered PEA_2PbI_4, 3D M0 and Rb5, and 3D/2D heterostructure (i.e., M0/2D and Rb5/2D) perovskite photovoltaics. The results are collected based on the average of 20–25 devices for each condition.[a]

Perovskites		**V_{OC} (V)**	**J_{SC} (mA/cm²)**	***FF* (%)**	**PCE (%)**
2D PEA_2PbI_4	Best	1.16	2.07	63.69	1.53
	Average	(0.99 ± 0.08)	(2.17 ± 0.2)	(57.15 ± 10.55)	(1.22 ± 0.21)
M0	Best	1.15	22.39	71.42	18.47
	Average	(1.09 ± 0.05)	(22.74 ± 0.3)	(70.23 ± 2.86)	(17.46 ± 0.66)
Rb5	Best	1.17	22.99	72.3	19.48
	Average	(1.15 ± 0.02)	(22.85 ± 0.55)	(71.09 ± 1.34)	(18.61 ± 0.56)
M0/2D	Best	1.15	21.96	70.73	17.84
	Average	(1.12 ± 0.04)	(22.3 ± 0.51)	(68.95 ± 1.31)	(17.28 ± 0.35)
Rb5/2D	Best	1.17	22.82	75.02	20.02
	Average	(1.17 ± 0.01)	(22.9 ± 0.27)	(73.09 ± 1.04)	(19.5 ± 0.43)

[a]Top value represents the optimal device and the bottom value represents average with standard deviation.

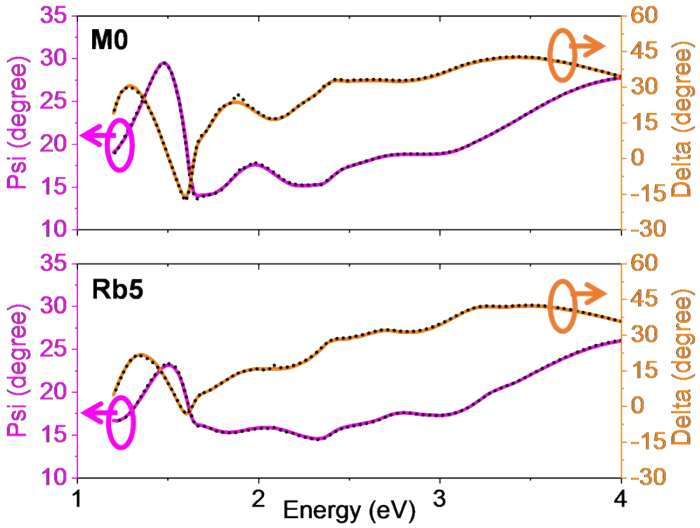

Thickness (nm)	M0	Rb5
Ellipsometry	405.8 ± 12.5	398.3 ± 9.7
Profiler	403.1 ± 8.7	402.9 ± 5.1

Fig. S1 Measured and simulated ellipsometry spectra for 3D M0 and Rb5 perovskite thin films. Table of summarized thickness for 3D M0 and Rb5 films measured by ellipsometry and profiler.

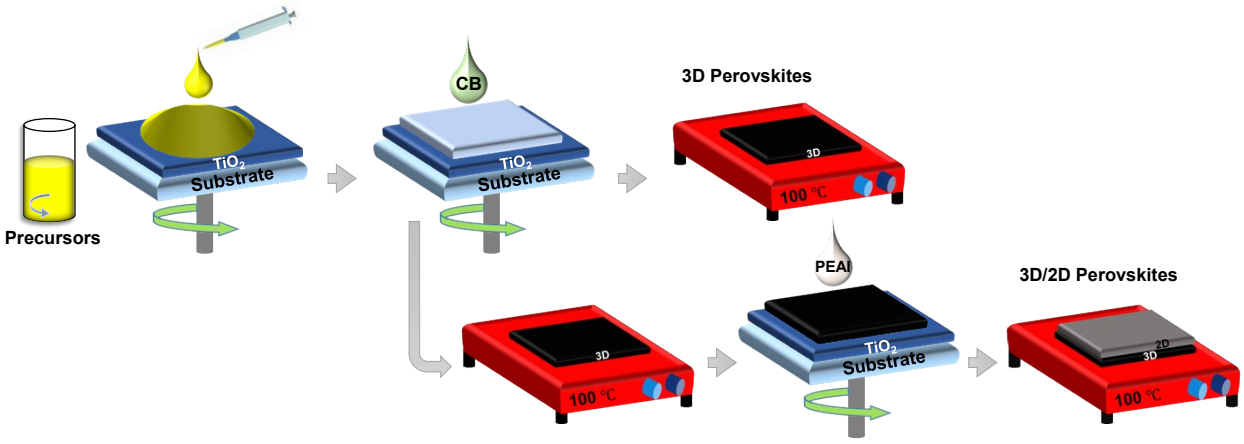

Fig. S2 Schematic representation of the deposition process for 3D and 3D/2D heterostructure perovskite solid-state thin films.

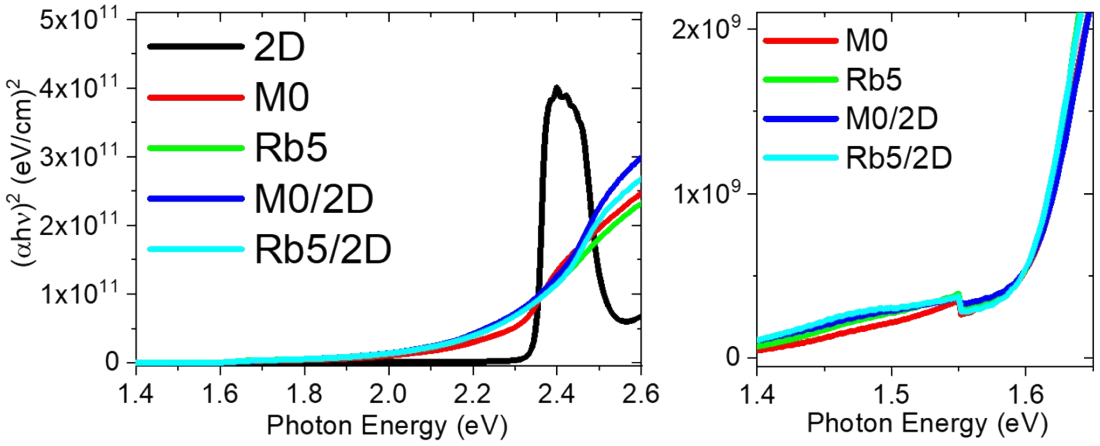

Fig. S3 Tauc plot of 2D layered PEA_2PbI_4, 3D M0 and Rb5, and 3D/2D heterostructure perovskite solid-state films.

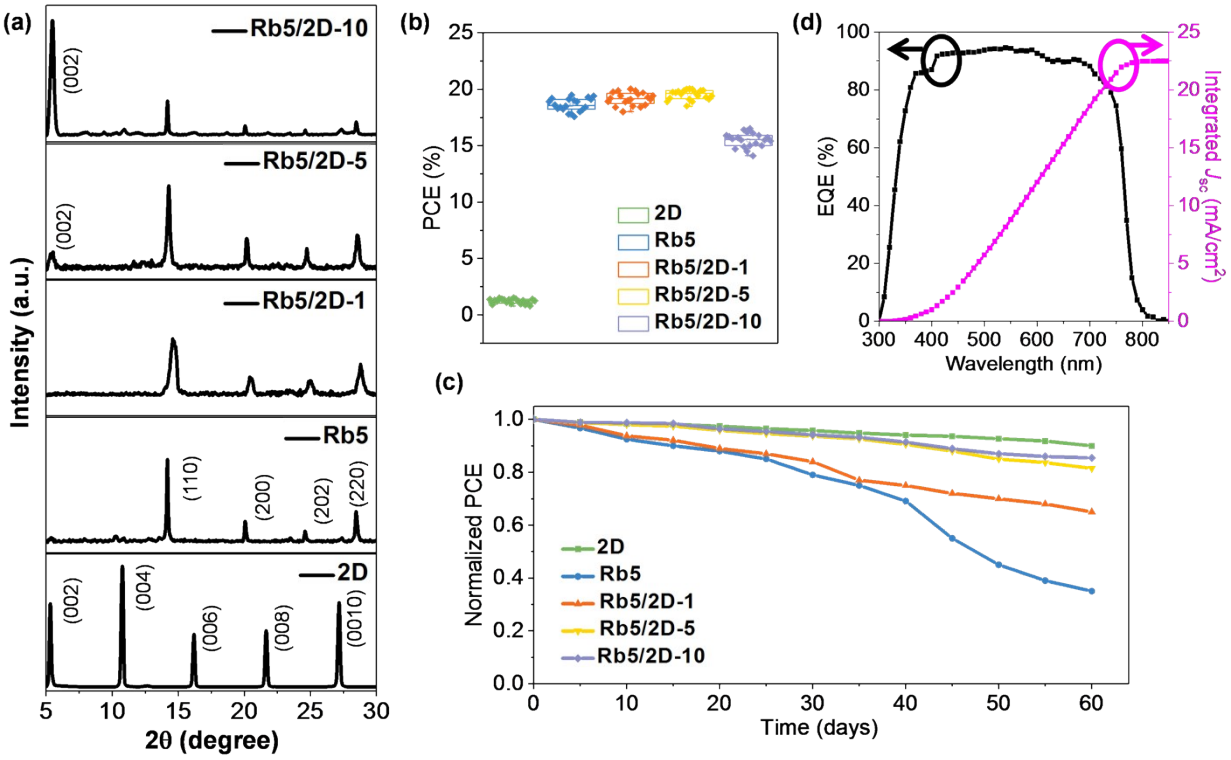

Fig. S4 Comparison of 2D layered PEA_2PbI_4, 3D Rb5, and Rb5/2D heterostructure perovskite films with various concentrations of the PEAI solution (1, 5, and 10 mg mL^{-1} in isopropanol). (a) XRD patterns. (b) Statistics of 20-25 perovskite solar cells. (c) Recorded long-term environmental

stability of corresponding perovskite solar cells exposed to an ambient environment with 50% relative humidity without encapsulation.

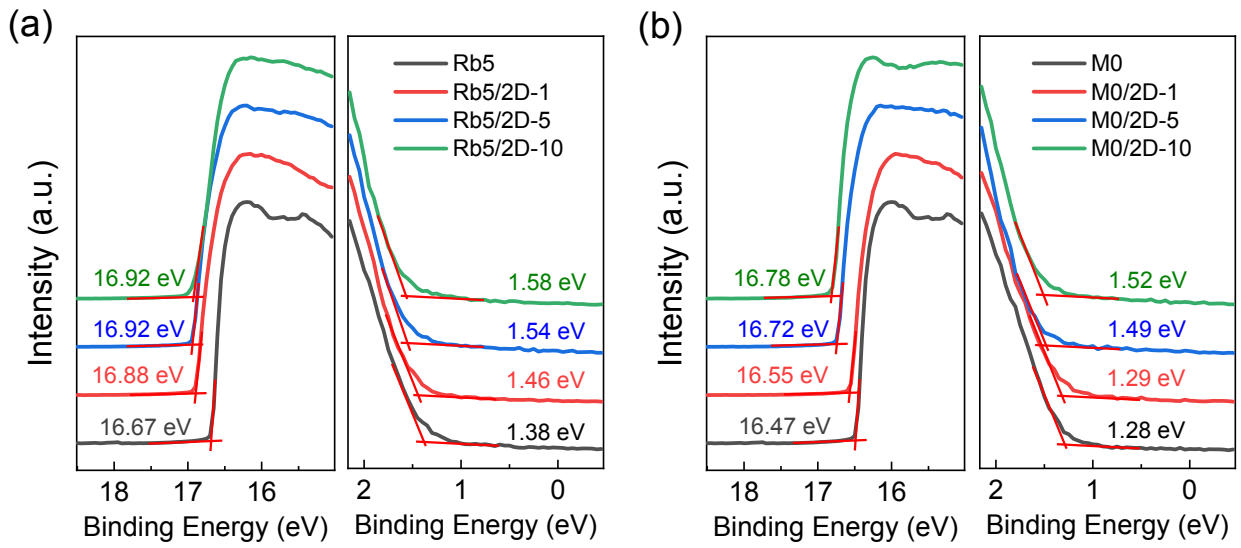

Fig. S5 UPS secondary electron edge (SEE) and the low binding energy region (near the Fermi energy E_F = 0 eV) of the classic 3D and 3D/2D bi-layer perovskites. The 2D layer thickness varies by 1 mg mL^{-1}, 5 mg mL^{-1}, and 10 mg mL^{-1} in isopropanol, respectively. The onset of ionization of filled states relative to zero binding energy is used to track the shifts of E_F relative to VBM.

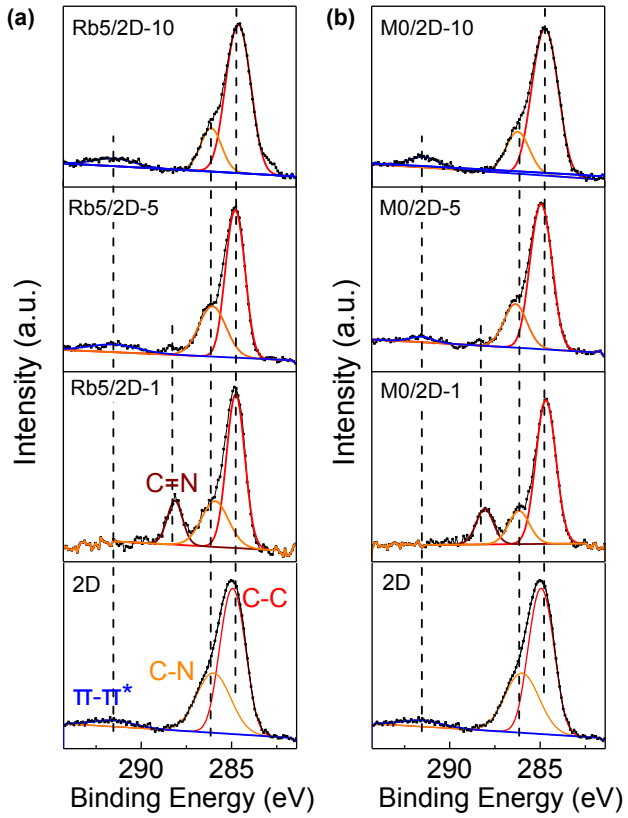

Fig. S6 Representative XPS core-level spectra of C 1s in (a) Rb5/2D and (b) M0/2D perovskite films. The Rb5 and M0 were post-treated by different concentrations of PEAI solutions, 1 mg mL^{-1}, 5 mg mL^{-1}, and 10 mg mL^{-1} in isopropanol. The y-axis is on a log scale to facilitate the view of the low-intensity peak.

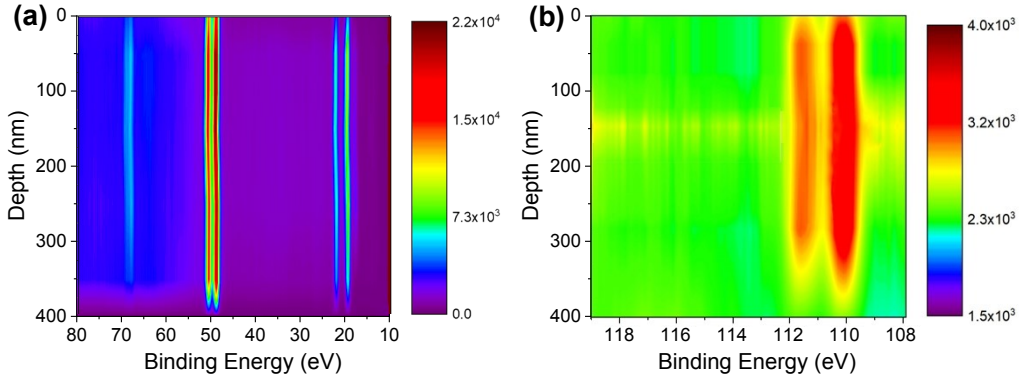

Fig. S7 (a) XPS depth profiling in the 80−10 eV range covering the Br 3d, I 4d, Pb 5d core level peaks in Rb5 film. (b) XPS depth profiling of Rb 3d in the Rb5 film.

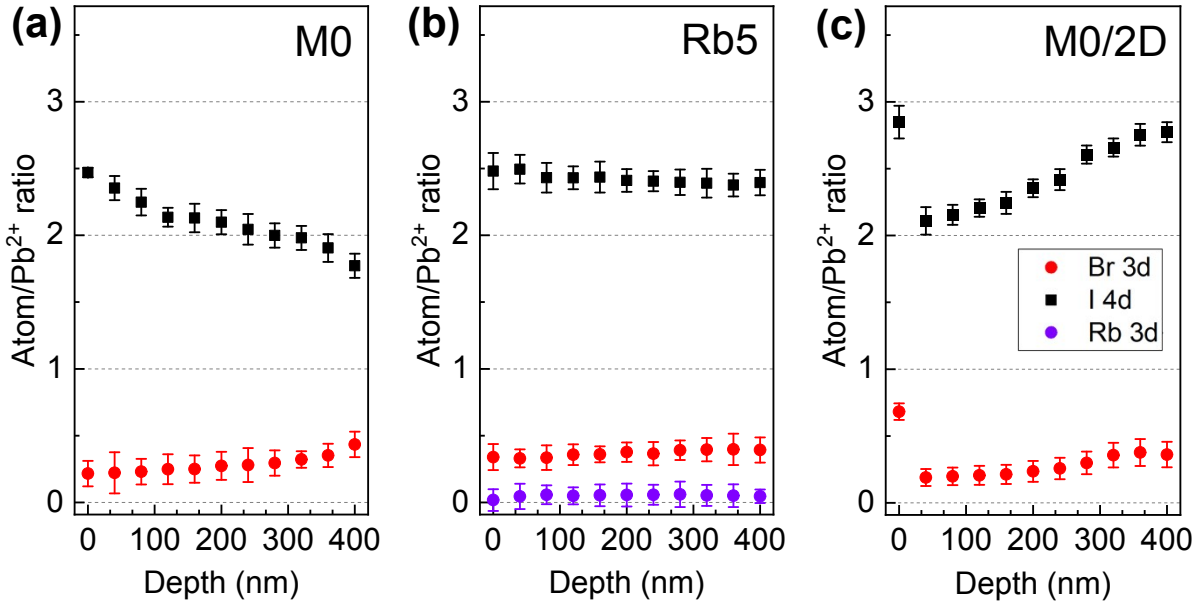

Fig. S8 The atomic ratios of the halides and alkali metal cations relative to lead Pb^{2+} in M0 (a), Rb5 (b), and M0/2D (c). Error bars indicate the standard deviation from averaging the results obtained with different spots.

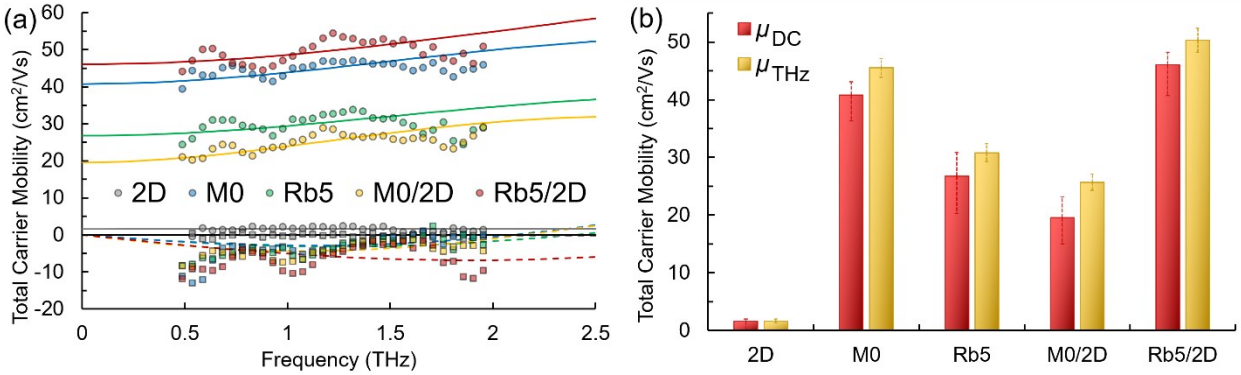

Fig. S9 800 nm photoexcitation (1.21 mJ/cm² for all samples except 3.31 mJ/cm² for 2D layered PEA_2PbI_4) TRTS results analogous to 400 nm photoexcited data shown in Figure 5 of the main text. (a) Frequency-dependent mobility extracted for each sample. Circles/solid line fits and squares/dashed line fits represent the real and imaginary components of the photoinduced

dielectric response, respectively. (b) μ_{DC} and μ_{THz} extracted from each frequency-dependent result in (a). Error bars in (b) represent 95% confidence interval limits for each value.

Broadband near band-edge 800 nm photoexcitation frequency-dependent conductivity (**Figure S9**) is used to determine mobility using a convolution of the sample's absorbance (directly measured using the photoexcitation pulse *in situ*) and the relative EQE at each wavelength, yielding a weighted average of 12.5 %. Each sample is assumed to have a similar EQE profile, which is a more tenuous assumption than using above-gap excitation in the center of its nominal range. The samples are also assumed to be 400 nm thick (does not influence mobility determination). The sample absorbs less than 15 % of the incident photoexcitation pulse, and so the entire sample depth is photoexcited to a near-uniform carrier density of 3×10^{17} to 7×10^{17} charge pairs/cm^3 and approximately an order of magnitude lower density than with 400 nm photoexcitation. The 800 nm results in **Figure S9** were collected 42 days after exposure to dry air (O_2 present but excluding H_2O and light). Additional 400 nm data (not included) suggested that Rb5 and M0 exhibited a ≈50 % reduction in mobility over this timeframe compared to earlier 400 nm photoexcitation experiments.

The mobility derived from **Figure S9** for each perovskite film is not within error, but there is also no systematic trend to suggest that the presence of Rb^+ or the 2D layered PEA_2PbI_4 has a substantial effect on mobility (i.e., the difference in mobility of each perovskite sample occurs without a particular pattern). We find the trend in mobility to be Rb5/2D > M0 > Rb5 ≈ M0/2D >> 2D. Compared to the 400 nm excitation mobility values, each mobility is two to three times higher (except 2D layered PEA_2PbI_4). This can be explained by order of magnitude lower carrier density (carriers are more mobile when less densely populated) and perhaps interrogation of the whole layer diluting the effect of heterogeneously distributed defects. It is also difficult to rule out possible two-photon absorption effects (given the strong absorbance and EQE at 400 nm) as playing a role in these differences as no fluence-dependent analysis was performed.

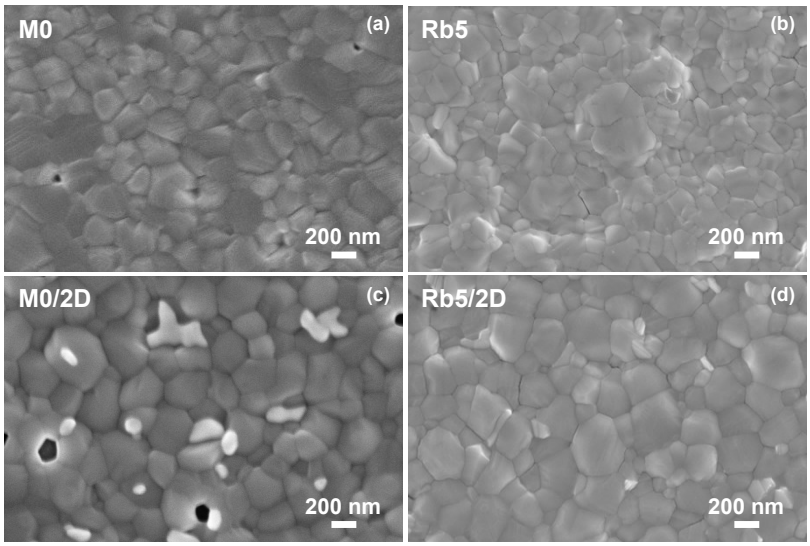

Fig. S10 Comparison of top-view SEM images and the horizontal scale bar is 200 nm. (a, b) 3D (i.e., M0 and Rb5) and (c, d) 3D/2D (i.e., M0/2D and Rb5/2D) perovskite solid-state thin films.

Table S3. Parameters determined from the Drude-Smith model fits from 400 nm and 800 nm TRTS datasets and extracted μ_{DC} and μ_{THz} mobility values. 95% confidence interval values for each parameter and mobility are indicated by parenthetical values (nonlinear) or those following +/- (linear).

Sample	**Rb5**	**M0**	**M0/2D**	**Rb5/2D**	**2D**
400 nm C_σ^*	0.903 *(---)*	1.08 *(---)*	1.00 *(---)*	1.42 *(---)*	100*** *(---)*
400 nm τ (fs)	46.8 *(28.4 – 70.6)*	40.0 *(23.3 – 62.1)*	45.5 *(24.9 – 63.5)*	31.8 *(15.8 – 61.6)*	0.48*** *(0 – 100)*
400 nm c_1	-0.686 *(-0.773 – -0.621)*	-0.692 *(-0.759 – -0.643)*	-0.734 *(-0.794 – -0.689)*	-0.736 *(-0.777 – -0.688)*	-0.979 *(-0.988 – -0.875)*
400 nm μ_{DC} (cm^2/Vs)	16.3 *(11.6 – 19.2)*	16.5 *(12.4 – 19.0)*	15.2 *(11.1 – 18.9)*	14.9 *(9.3 – 17.2)*	1.3 *(0.3 – 1.6)*

400 nm μ_{THz}	21.7 *+/- 1.5*	21.2 *+/- 1.3*	21.8 *+/- 1.3*	18.8 *+/- 1.5*	1.1 *+/- 0.3*
800 nm C_σ**	1.17 *(0.68 – 366)*	2.31 *(1.54 – 11.3)*	1.15 *(0.70 – 26.3)*	2.82 *(1.48 – 520)*	164*** *(---)*
800 nm τ (fs)	42.6 *(16.7 – 70.3)*	36.4 *(24.8 – 53.1)*	44.8 *(23.1 – 64.2)*	25.7 *(15.5 – 44.4)*	0.1*** *(0 – 155)*
800 nm c_1	-0.643 *(-0.717 – -0.578)*	-0.602 *(-0.642 – -0.556)*	-0.684 *(-0.733 – -0.634)*	-0.646 *(-0.723 – -0.605)*	-0.988 *(-0.990 – -0.986)*
800 nm μ_{DC} (cm^2/Vs)	25.1 *(19.0 – 28.9)*	40.0 *(35.7 – 42.3)*	19.6 *(15.6 – 23.1)*	45.5 *(40.2 – 47.6)*	1.7 *(0 – 2.0)*
800 nm μ_{THz}	30.8 *+/- 1.6*	45.5 *+/- 1.6*	25.7 *+/- 1.4*	50.3 *+/- 2.1*	1.7 *+/- 0.34*

*,** C_σ are ($\times 10^{5,\ **4}$) and are meant to convey relative conduction/mobility; however, they are not explicitly corrected for sample absorption (or slight pump power fluctuations) here.

*** Values for 2D reached hard-limits set for the model and tend towards ∞ for C_σ and 0 for τ.

References

1. A. J. Biacchi, S. T. Le, B. G. Alberding, J. A. Hagmann, S. J. Pookpanratana, E. J. Heilweil, C. A. Richter and A. R. Hight Walker, *ACS Nano*, 2018, **12**, 10045-10060.
2. J. C. Speros, H. Martinez, B. D. Paulsen, S. P. White, A. D. Bonifas, P. C. Goff, C. D. Frisbie and M. A. Hillmyer, *Macromolecules*, 2013, **46**, 5184-5194.